MDPI

Article

Experimental Investigation of Frictional Resistance in Sliding Contact between Undulating Surfaces and Third-Body Particles

Qiang Li * and Markus Heß

Department of System Dynamics and Friction Physics, Technische Universität Berlin, 10623 Berlin, Germany; markus.hess@tu-berlin.de
* Correspondence: qiang.li@tu-berlin.de

Abstract: The third-body particle-involved sliding contact between two rough rubbers with wavy surfaces is experimentally studied. The experiment is designed to isolate the direct contact between the first bodies so that friction resistance is induced completely by the interactions between the third-body particle and the surfaces of the rubbers. In dry contact of a single particle, it is found that the particle exhibits pure rolling during the sliding of the first bodies, and the macroscopic friction resistance for overcoming sliding does not depend on the particle size, but it is significantly influenced by the initial position of the surface waviness relative to the particle's position. The behavior of the particle under lubricated conditions exhibited significant differences. Due to the low local friction at the interface, the particle rapidly glided down to the valley of the waviness during compression. This abrupt motion of the particle resulted in it coming to rest in a stable position, awaiting a substantial force to push it forward. The friction resistance in the case with lubrication was found to be independent of the initial position of the waviness, and its value consistently remained at the maximum found in dry contact. Therefore, lubrication actually increases the macroscopic friction resistance. An approximate solution for the specific case of dry contact is proposed to understand the friction behavior.

Keywords: friction; third body; contact mechanics; particle; wavy surface

1. Introduction

The immediate interface, including layers and wear particles, often referred to as the "third body", plays a significant role in determining tribological properties [1,2]. However, due to the intricate nature of tribological processes at this interface—encompassing friction, adhesion, material transfer, debris formation, mechanical intermixing, phase transformations, oxidation, and corrosion—empirical methods have primarily been employed in studying the third-body contact problem [3–5]. Frequently, coefficients of friction and wear rates are measured while controlling macroscopic parameters like loading, velocity, temperature, and environmental conditions [6–8]. When studying complex tribological systems, results often yield unpredictability and sometimes conflicting observations. For example, certain sliding experiments have shown significantly lower wear rates in three-body abrasive sliding compared to two-body contact [9], while in other scenarios higher friction and wear are reported [10]. These disparities largely arise from the different roles played by particles during sliding. In some instances, wear particles engage in rolling motion at the interface, whereas in others, hard wear debris accumulates in the wear track, resulting in increased friction resistance. In a recent molecular dynamics simulation, a transition from particle rolling to a shear band-like state during the sliding was observed [11]. Additionally, the loading conditions and particle size can influence friction properties. For example, it was found that repeated reciprocated sliding promotes the formation of a third body that stabilizes the friction compared to non-repeated sliding [12]. In a braking system, larger particle sizes can improve the motion stability of the system [13].

To gain a fundamental understanding of the role of the third body, it is logical to isolate some effects and focus on some specific ones in a more controlled manner. For instance, recent research concentrated on the sliding contact between just two asperities, successfully establishing criteria for transitioning from plastic smoothing to wear particle formation [14]. Recent experiments have investigated the dynamic friction between two sliding surfaces with particles positioned between them, focusing on particle transport while excluding consideration of first-body contact [15,16]. Other studies [17,18] have focused on the interactions between particles and substrate under dry and wet condition, while [19] investigated the influence of lubrication based on a three-body contact. In this paper, we conduct an experimental study in a "pure form" from the perspective of contact mechanics.

The present work aims to study the role of third-body particles in sliding contact between two rough surfaces. To achieve this, the experiment is designed to avoid direct contact between the first bodies. Therefore, the sliding friction is induced completely by the interaction between the existing particles and the surfaces of the first bodies. Moreover, the particles are much harder than the substrates (rubbers), and the sliding is carried out at low velocity, rendering wear negligible. The rough surfaces are modelled by one-dimensional waviness with a small amplitude. Experiments under dry conditions and with a lubricant are conducted to study the influence of the local friction. Furthermore, the effects of particle size, particle number, and the sliding velocity on the macroscopic friction are investigated. Finally, an approximate model is discussed for analyzing the forces acting on the particles.

2. Experiment Method

An experimental setup based on the construction for an adhesive test described in [20] was further developed to investigate the contact of third-body particles. As shown in Figure 1a, one of the elastomer bodies with a wavy surface (located below) is positioned on a transparent glass, while the other (above) is affixed to a 3D force sensor, which is connected to linear stages. Two linear stages are used to control both the vertical and horizontal movement of the upper elastomer. A rotation stage is positioned beneath the lower elastomer for conducting rotation tests. A camera is situated below the rotation stage to monitor the movements of the particles. Some components of the setup were fabricated using a 3D printer to facilitate adjustments in the installation process.
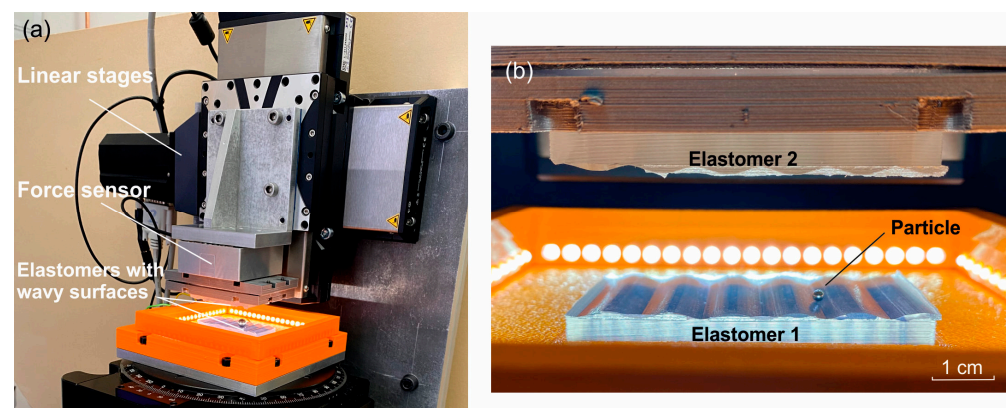

Figure 1. (**a**) Experimental setup for studying the sliding contact of third-body particles. (**b**) Elastomer samples with wavy surfaces and an interposed steel particle.

Figure 1b presents a more detailed view of the contact region. The elastomers with one-dimensional wavy surfaces were cast out of transparent silicone rubber (TFC Silicon Rubber Type 19). These elastomers have an elastic modulus of approximately 0.9 MPa and ultimate tensile strength of 2.5 MPa. Each elastomer block has dimensions of 60 mm by 30 mm, with a thickness of about 12 mm, plus the added waviness. The molds used in the production were created using 3D printing technology with high resolution. The particles

used in the experiments are simple steel balls with diameters ranging from 2 mm to 5 mm, and they are much harder than the elastomers. The steel balls have a surface roughness of approximately 0.13 μm, which is significantly smoother than the rubber (about 2.56 μm).

The experiment involving the sliding contact of two identical wavy surfaces with particles between them was conducted. As shown in Figure 1b, the transparent elastomer below was securely affixed to a glass plane, and particles were positioned within the valleys of the surface waviness. Subsequently, the upper elastomer was aligned to be parallel to the lower one and adjusted to a position of zero clearance. In this configuration, the gap between the peaks of the two wavy surfaces was set at *zero*, eliminating any tangential frictional forces caused by the elastomers. Consequently, the frictional resistance is completely induced by the presence of the third-body particles.

Several factors may significantly affect the sliding contact, including the geometry of the surface waviness (amplitude and wavelength), the size and quantity of particles, and the phase shift between the two wavy patterns ΔL, as illustrated in Figure 2. The results shown in the next section will show that this phase shift plays an important role in determination of the macroscopic friction resistance.
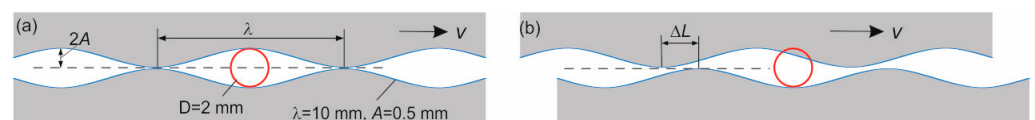

Figure 2. (**a**) Illustration of the particle and gap between two wavy surfaces. The initial positioning of the upper elastomer (representing the phase shift between the two wavy patterns) is a crucial factor in sliding contact, as shown in (**b**).

The following results pertain to scenarios with surface waviness characterized by a small amplitude (A) of 0.5 mm and a large wavelength (λ) of 10 mm. The steel balls employed vary in diameter (D) and are listed in Table 1, ranging from 2 mm to 5 mm. In most cases, the sliding velocity of the upper surface is very low, at 0.05 mm/s. The upper elastomer is moved tangentially by a distance of 40 mm (equivalent to 4λ), and only one particle is placed between the elastomers. The influence of parameters such as the number of particles, sliding velocity of the upper elastomer, and lubrication conditions will be discussed in the subsequent sections of this paper. The experiment series is shown in Table 2.

Table 1. Factors considered in the experiment.

Factor	Value
Geometry of the wavy surface	Amplitude A = 0.5 mm, wavelength λ = 10 mm
Particle size (Diameter of the steel ball)	D = 2, 2.38, 3, 3.18, 4, 4.5, 4.76, 5, 5.56 mm
Particle number	1, 2, 3, 4, 6, 8
Initial position of the upper rubber	Phase shift $\Delta L/\lambda$ = 0, 0.2, 0.4, 0.6 0.8, 1
Sliding velocity of the upper rubber	0.05, 0.1, 0.2, 0.4, 0.8 mm/s
Lubricant	Without and with (SHC XMP-320)

Table 2. Experiment series.

Experiment series 1: Influence of particle size and phase shift ('✓'—conducted; '×'—not conducted)								
$\Delta L / \lambda$	D = 2 mm	2.38	3	3.18	4	4.5	4.76	5	5.56
0				✓					✓
0.2				✓					×
0.4				✓					×
0.6				✓					×
0.8				✓					×
1				✓					×

Other conditions: single particle, without lubricant

Experiment series 2: Influence of particle number

Particle number: N = 2, 4, 6, 8

Other conditions: v = 0.05 mm/s, $\Delta L / \lambda$ = 0, without lubricant

Experiment series 3: Influence of sliding velocity

Sliding velocity: 0.05, 0.1, 0.2, 0.4, 0.8 mm/s

Other conditions: single particle D = 2 mm, $\Delta L / \lambda$ = 0, without lubricant

Experiment series 4: Influence of lubricant

Phase shift: $\Delta L / \lambda$ = 0, 0.2, 0.4, 0.6, 0.8

Other conditions: single particle D = 3 mm, v = 0.05 mm/s

3. Experimental Results

To attain fundamental insights, the experiment was started with the case of a single particle, and the focus was on the influence of the particle size and the phase shift between two undulating surfaces during slow sliding (experiment series 1 in Table 2). Then, the effects of the particle number and the sliding velocity (experiment series 2 and 3) as well as the influence of lubricant (experiment series 4) were investigated.

3.1. Sliding with a Single Particle under Dry Contact Condition

During the experiment, a particle was positioned within the valley of the wavy surface on the lower elastomer. Subsequently, as depicted in Figure 2, the upper elastomer was controlled to move vertically until reaching zero clearance. Once in this position, the upper elastomer underwent a very slow tangential movement of 40 mm (4λ).

Figure 3 presents the measured normal and tangential forces for a single particle, with diameters of D = 2 mm (blue), D = 3 mm (red), and D = 4 mm (purple). There are two interesting phenomena observed as follows:

(1) In all of these cases, the normal and tangential forces exhibit periodic changes with a period equal to two times the wavelength of the surface waviness (2λ), which is half the distance the upper rubber moves. Hence, it can be deduced that the steel sphere undergoes almost pure rolling during the sliding of the rubber. This conclusion is supported by images captured during the experiment, as shown in Figure 4, where the particle clearly moves a distance of 2λ. Therefore, it can be inferred that the local coefficient of friction is significantly high, and the particle experiences pure rolling in the sliding process.

(2) Another notable phenomenon is the influence of particle size and the phase shift between the two wavy surfaces. Figure 3a shows the results of the case with a phase shift of $\Delta L / \lambda$ = 0 (as illustrated in Figure 2a). Both the normal and tangential forces undergo harmonic changes. When using larger particles, there is an increase in the mean normal force and the amplitude of oscillation for both the normal and tangential forces. However, in the case with a phase shift of $\Delta L / \lambda$ = 0.6, as shown in Figure 3b, the forces exhibit non-harmonic variations, and the amplitude is notably reduced. Interestingly, in both cases,

the fluctuation of the ratio of the normal and tangential forces (F_x/F_z) remains relatively consistent during the sliding, even when employing different sizes of particles.
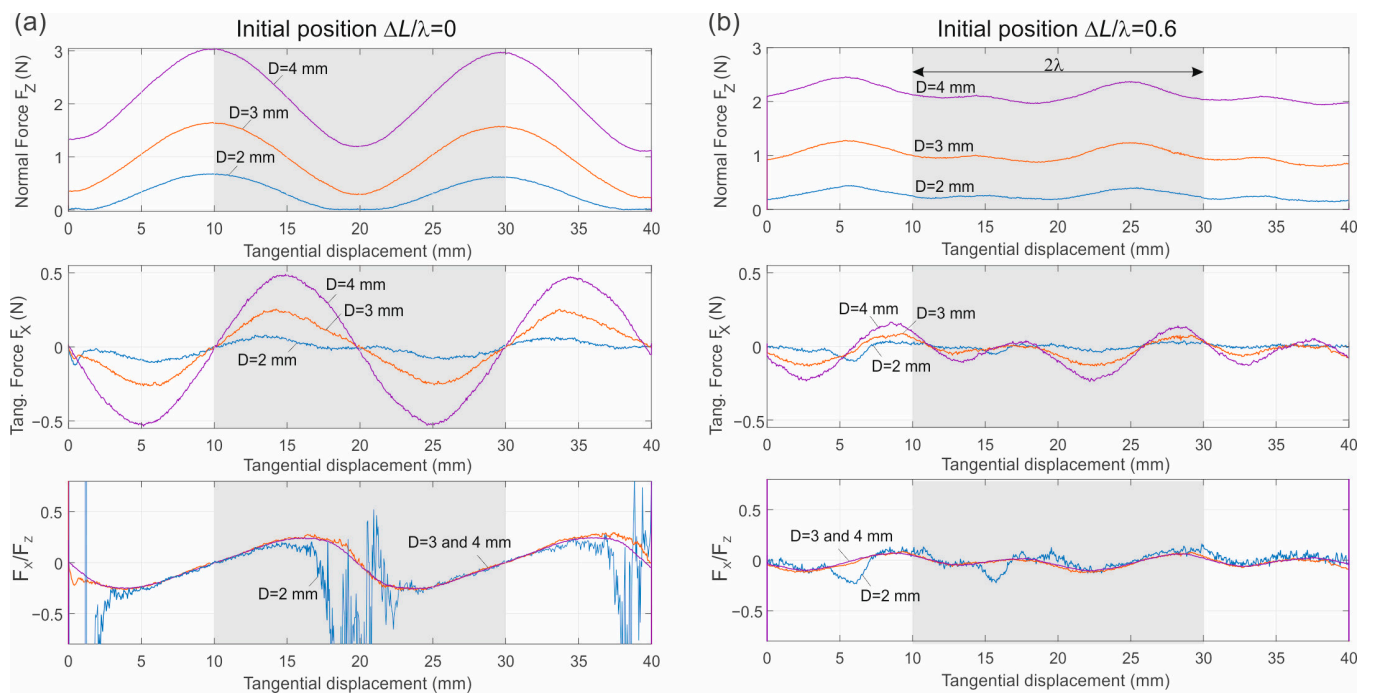

Figure 3. Measured normal and tangential forces during sliding contact for particles D = 2 mm (blue), 3 mm (red), and 4 mm (purple). The left panel (**a**) shows the case without phase shift between two wavy surfaces as illustrated in Figure 2a, and the right one (**b**) shows the case with a phase shift.
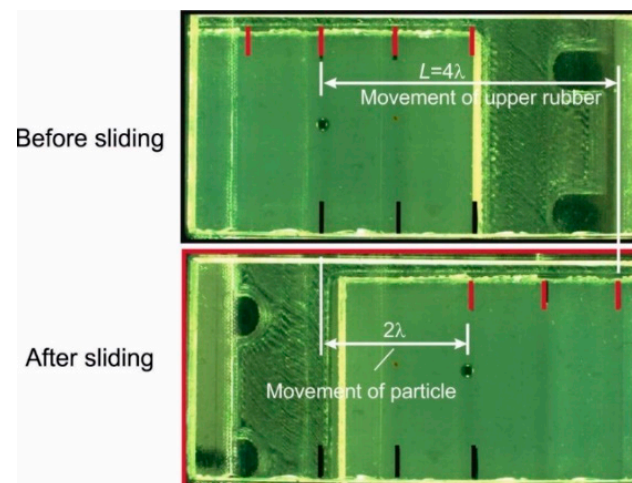

Figure 4. Images of the contact region before and after sliding. The black bars indicate the fixed (lower) rubber and the red bars the movement of the upper rubber.

The maximum ratio of the normal and tangential forces is a critical parameter characterizing the friction resistance during sliding. Figure 5 shows the mean normal force (a), the amplitude of normal force fluctuation (b), the maximum tangential force (c), and the friction resistance (d) with higher values of particle size and phase shift, as listed in Table 1. It is worth noting that the initial position of the upper rubber significantly affects the fluctuation of forces; this fluctuation is smaller when the wavy surfaces are initially arranged such that the peak of the upper rubber aligns with the valley of the lower rubber (cases of $\Delta L/\lambda$ = 0.4 and 0.6). Focusing on friction resistance, as presented in Figure 6, it is

apparent that it strongly depends on the phase shift between the two wavy surfaces but has only a slight dependence on the size of the particles.
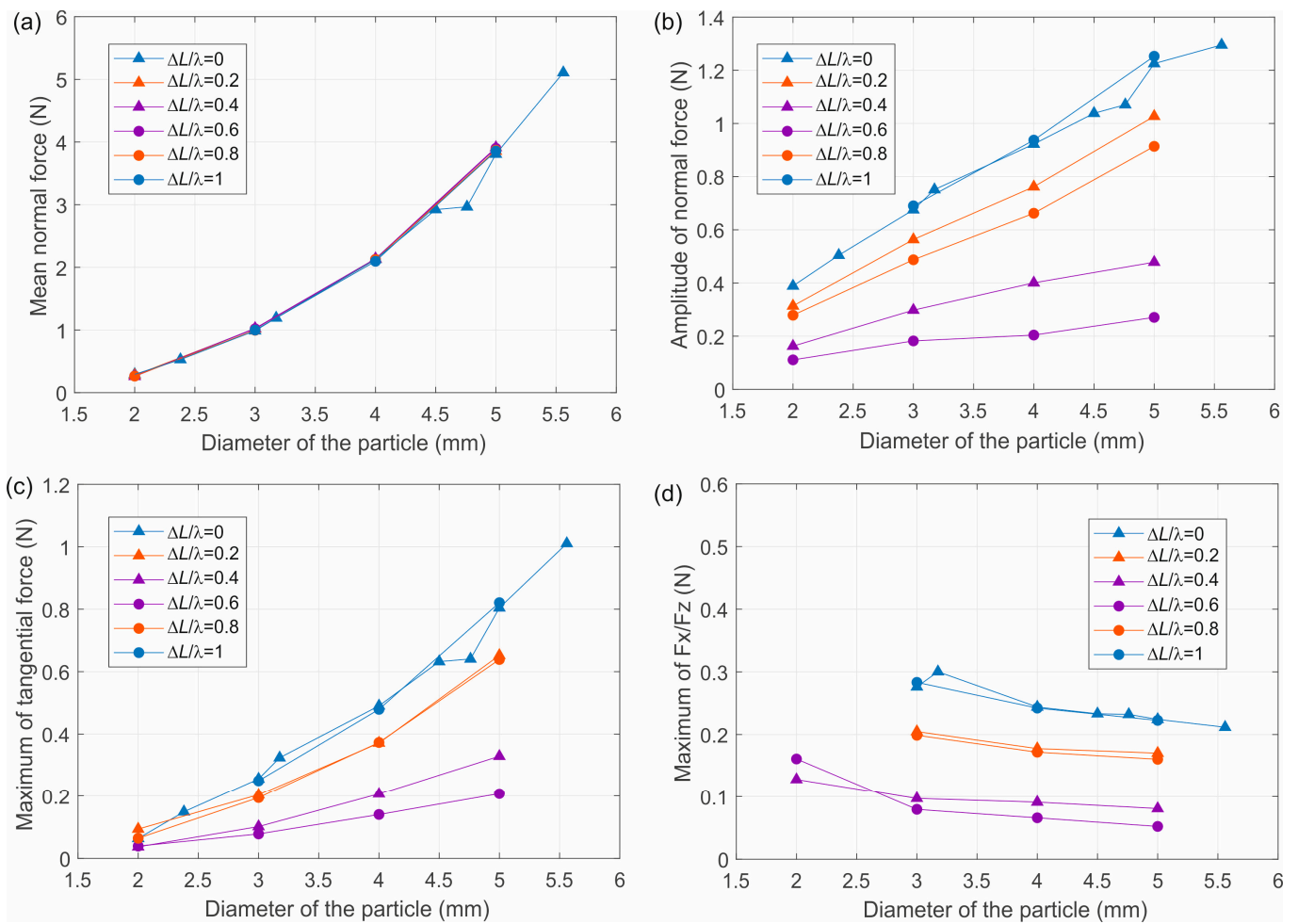

Figure 5. Dependence of (**a**) the mean normal force, (**b**) amplitude of the normal force, (**c**) the maximum of the tangential force, and (**d**) the frictional resistance on the particle size and the initial position of the upper rubber (phase shift between two wavy surfaces).
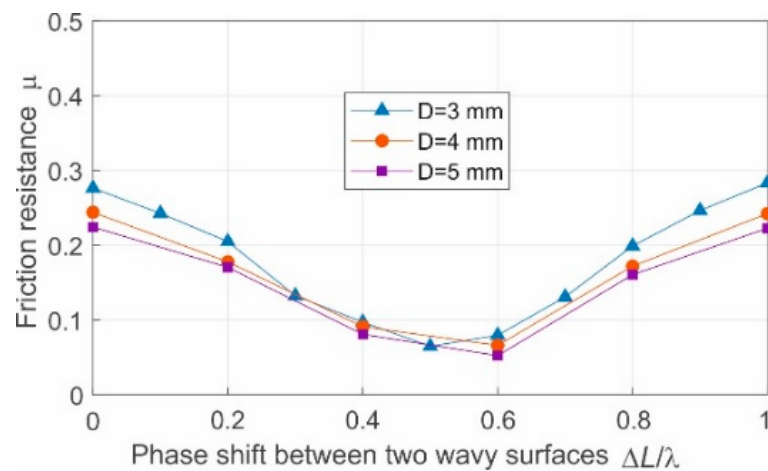

Figure 6. Dependence of the friction resistance on the initial position of the upper body in dry contact. The friction is very slightly dependent on the particle size.

The particle undergoes rolling on the rubber surface during the process, and it is much harder than the rubber. As a result, the wear is minimal. Moreover, the measurement of the rubber roughness after the test indicates no difference in roughness.

3.2. Influence of the Particle Number and Sliding Velocity

The number of particles and the sliding velocity of the upper rubber are also potential factors that can affect the sliding contact. Figure 7a shows results with a few particles, all with the same diameter (D = 2 mm), and in this case, the phase shift was zero. During the experiment, the particles were sparsely positioned in the valleys of the surface waviness and did not interact with each other while rolling. It is evident that, under these conditions, the number of particles impacts only the amplitude of the forces, while the friction resistance remains constant.
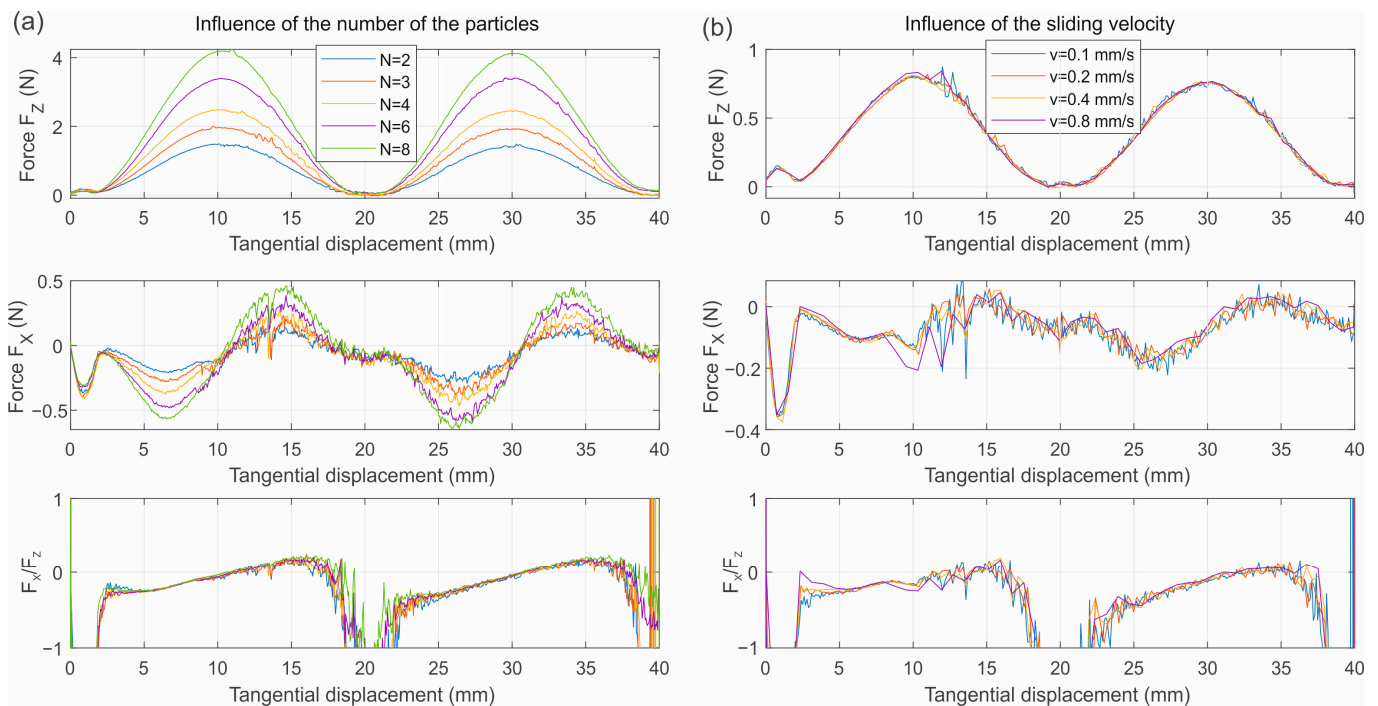

Figure 7. Influence of the particle number (**a**) and the sliding velocity of the upper rubber (**b**). In these experiments, the phase shift is zero and the particle size is D = 2 mm.

Figure 7b presents the results at different sliding velocities of the upper rubber for a single particle with a diameter of 2 mm and zero phase shift. Within the range of 0.05 to 0.8 mm/s, no discernible influence on the sliding contact was observed.

3.3. Influence of Lubrication

The aforementioned experiment indicates that the particle undergoes nearly pure rolling between the two rubber surfaces during sliding, suggesting that the local coefficient of friction can be considered quite high. To explore scenarios with small local friction, lubricant (SHC XMP-320) was introduced into the interface between the rubber surfaces, and the sliding experiment was repeated using particles with a size of D = 3 mm and various initial positions of the upper rubber (experiment series 4). The sliding velocity was small (v = 0.05 mm/s). The resulting forces are depicted in Figure 8.
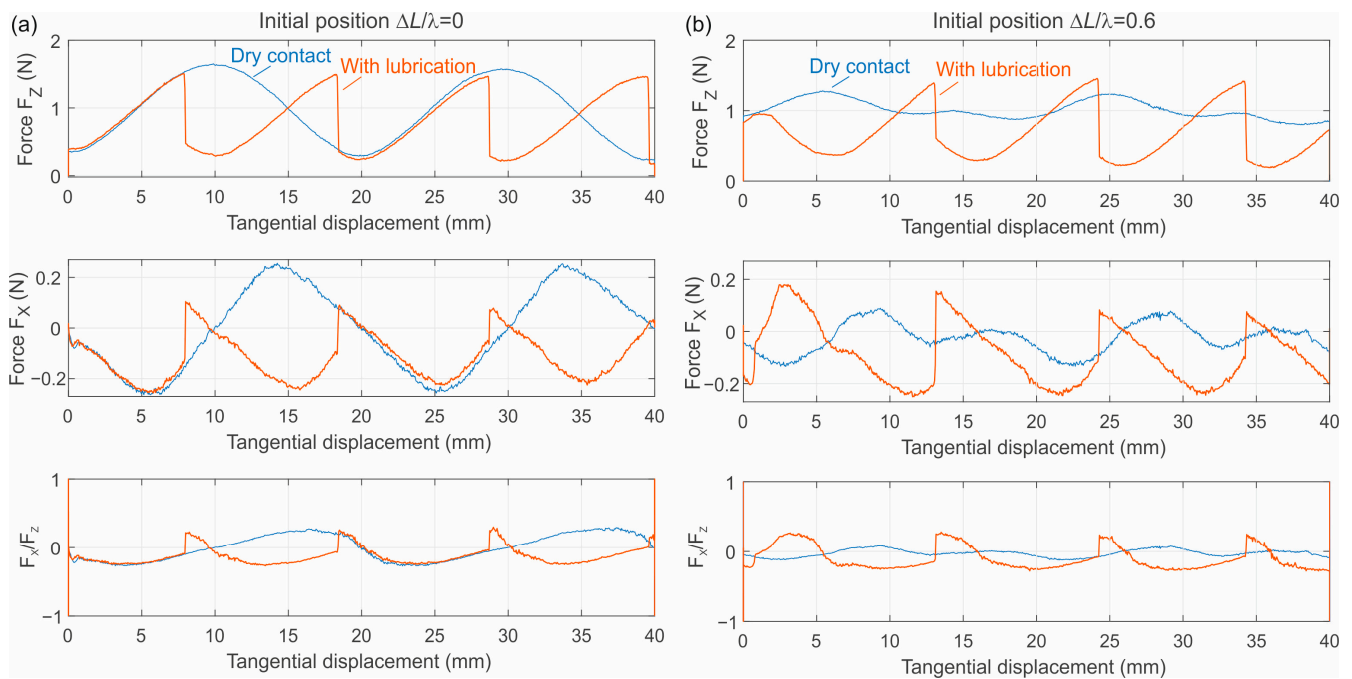
Figure 8. Experimental results with particle D = 3 mm under the condition of lubrication (red) for (**a**) phase shift $\Delta L/\lambda = 0$ and (**b**) $\Delta L/\lambda = 0.6$.

In comparison to the dry contact, a distinct phenomenon emerges: when pushed by the wavy surface of the upper rubber, the particle climbs (rolls) along the surface of the lower rubber, ascending to the peak of the surface. During this phase, the compression force is notably high, and there may be minimal lubrication between the particle and the rubber. Subsequently, the particle rapidly glides down to the valley of the waviness due to the reduced friction provided by the lubricant. As a result of this slip effect, the initial position of the upper rubber becomes less significant. Thus, the red curves in Figure 8a,b for the lubricated cases are quite similar. Regarding friction resistance, it remains almost consistent across all initial positions, as shown in Figure 9. It is noted that a jump occurred occasionally at positions slightly different from those shown in Figure 8.
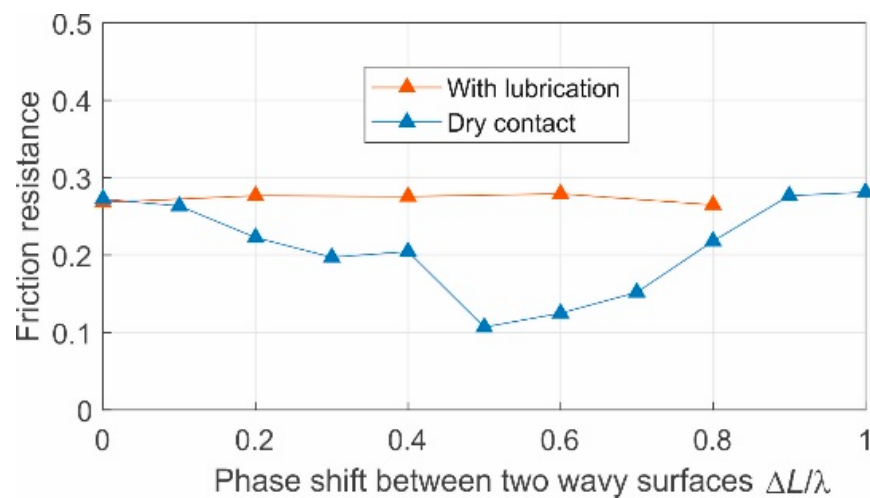

Figure 9. Friction resistance under conditions of dry contact (blue) and with lubrication (red). The particle size is D = 3 mm.

In the case with lubrication, particle transport differs from that in dry contact. The presence of lubricant facilitates faster particle movement, primarily as the particle glides down the waviness. The period of horizontal particle movement remains at 4λ, the same as the movement of the upper rubber.

4. An Approximate Solution for the Case without Phase Shift

We briefly discuss the contact properties of the particle. The coordinate system is defined as shown in Figure 10a. The profile of the lower and upper bodies can be described as follows

$$z_1(x) = -A\left[\cos(2\pi x/\lambda) + 1\right], \tag{1}$$

$$z_2(x) = A\left[\cos(2\pi(x + \Delta L - u_x)/\lambda) + 1\right]. \tag{2}$$

where A and λ are the amplitude and wavelength of the waviness, ΔL is the phase shift as shown in Figure 2b, and u_x is the horizontal movement of the upper body. The function of the gap between the two surfaces is then

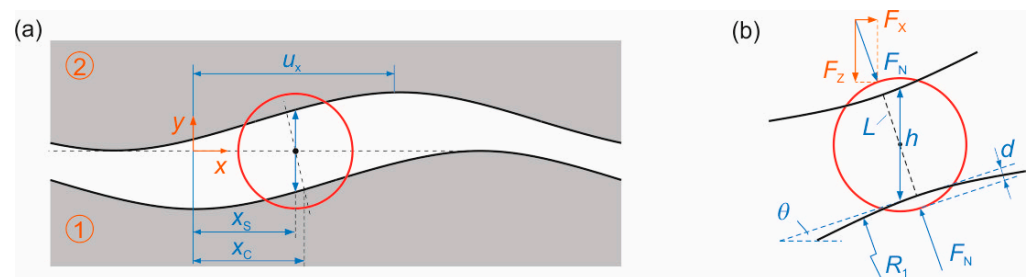$$h(x, \Delta L, u_x) = 2A - A[\cos(2\pi(x + \Delta L - u_x)/\lambda) + \cos(2\pi x/\lambda)]. \tag{3}$$

Figure 10. (**a**) Illustration of particle's position between two waviness profiles with $\Delta L = 0$. The upper body undergoes horizontal movement u_x, while the position of the particle is approximately $x_s = u_x/2$ and the position of contact point is denoted as u_C; (**b**) Parallel loading on the particle from upper and lower surfaces.

If the spherical particle undergoes pure rolling during sliding, then the horizontal movement of the particle is approximately half that of the upper body ($x_s = u_x/2$) (Figure 10a). Thus, the gap can be expressed as a function of the distance of the upper body:

$$h(u_x, \Delta L) = 2A - A[\cos(2\pi(\Delta L - u_x/2)/\lambda) + \cos(\pi u_x/\lambda)]. \tag{4}$$

Observing the particle stuck between two curved surfaces, if there is no phase shift between the two waviness profiles, $\Delta L = 0$, then the tangents at the upper and lower interfaces at an arbitrary position are parallel. Therefore, the contacts at both surfaces are same, as shown in Figure 10b, and only normal loads F_N act on the particle (perpendicular to the tangent with an angle θ). The case with a phase shift $\Delta L \neq 0$ is much more complicated: where the particle is located in a "wedge", then tangential forces exist at the interface, dependent on the loading history. Here we analyze only the case $\Delta L = 0$.

We neglect the gravity of the particle and consider only the loading from the elastic bodies, employing the Hertzian contact theory. It is important to note that the assumptions in Hertzian contact theory do not fully align with experiment conditions: firstly, the elastomer was largely deformed during the sliding experiment, especially when the gap was very small; secondly, the size of the contact area may be comparable to the particle size, rendering the half-space assumption invalid. However, we still use Hertzian contact theory to provide an approximation under quasi-static conditions.

As depicted in Figure 10b, we treat the lower (or upper) contact as a contact between a rigid sphere with radius R and an elastic body with a two-dimensional radius of curvature R_1, elastic modulus E, and Poisson's ratio ν. The contact interface (tangent of the waviness)

at the center of the contact area $x = x_C$ (not the center of the particle x_S) at this moment is inclined to the x-coordinate by an angle θ. It is known that this contact is equivalent to contact between a rigid sphere with another effective radius R_e and an elastic half space. The effective radius in this case is given by

$$R_e = \sqrt{\left(\frac{1}{R_1} + \frac{1}{R}\right)^{-1} R} = R\sqrt{\frac{R_1}{R + R_1}} \tag{5}$$

with

$$R_1 = \frac{\left(1 + z_1'^2(x)\right)^{3/2}}{z_1''(x)} = \frac{\left(1 + \left(\frac{2\pi A}{\lambda}\sin\frac{2\pi x}{\lambda}\right)^2\right)^{3/2}}{\left(\frac{2\pi}{\lambda}\right)^2 A \cos\frac{2\pi x}{\lambda}}. \tag{6}$$

The distance in the normal direction between the upper and lower surfaces is defined as L, as shown in Figure 10b. Then, the indentation depth is equal to $d = R - L/2$. Following the Hertzian contact theory, the normal force is given by

$$F_N = \frac{4}{3}E^* R_e^{1/2} d^{3/2} = \frac{4}{3}E^* R_e^{1/2}(R - L/2)^{3/2}, \text{ at} x = x_c \tag{7}$$

For the small ratio of the amplitude and wavelength, in the case of experiment $\lambda/A = 0.05$, the difference between the gap h and the distance L is very small, with maximal difference of only 1.02% at the position $x_S = 0.235\lambda$ and 0.765λ. Therefore, one can use the gap h at the position at $x = x_S$ to replace the distance L at $x = x_C$ and also use the effective radius R_e at position $x = x_S$ instead of that at $x = x_C$. Substituting Equations (4)–(6) into (7), one can obtain the normal force as well as its components in the horizontal and vertical direction at $x = u_x/2$

$$F_X = F_N \sin\theta = \frac{4}{3}E^* R_e^{\frac{1}{2}}\left(R - \frac{h}{2}\right)^{\frac{3}{2}}\sin\theta \quad F_Z = F_N \cos\theta = \frac{4}{3}E^* R_e^{\frac{1}{2}}\left(R - \frac{h}{2}\right)^{\frac{3}{2}}\cos\theta. \tag{8}$$

The ratio of the horizontal and vertical force is simply equal to

$$F_X/F_Z = \tan\theta = z'(x = u_x/2) = 2\pi A/\lambda \sin(\pi/\lambda u_x). \tag{9}$$

This approximate solution with the same waviness $A = 0.5$ mm and $\lambda = 10$ mm is presented in Figure 11. The effective modulus was fitted to achieve good agreement with the vertical force F_Z, set as 0.6 MPa. It is observed that the analytical solution for the horizontal force is larger than the experimental results; however, they exhibit the same trend. The horizontal force changes non-harmonically. As shown in Equation (9), the macroscopic friction is independent of the particle size and the elastic modulus of the bodies, and the maximal value is $2\pi A/\lambda$, which is equal to 0.314 in the case of $A = 0.5$ mm and $\lambda = 10$ mm, and slightly larger than the experimental observation. Although the experimental conditions do not fully coincide with the assumptions in the Hertzian theory, the solution (9) still provides a good approximation to the maximal friction resistance in this case.
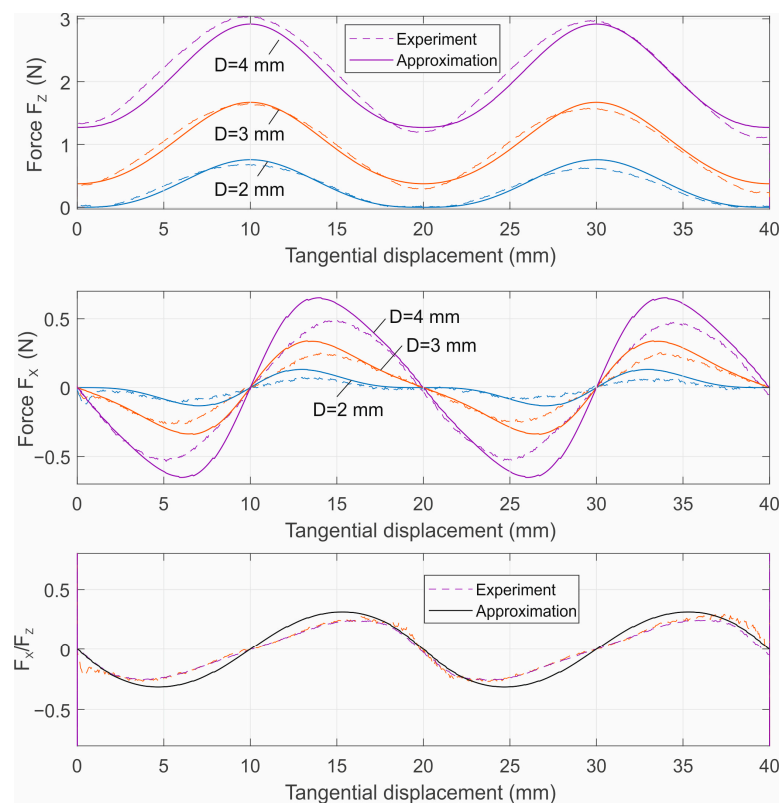
Figure 11. The approximate solution according to Equations (7)–(9) for the case $\Delta L = 0$ (solid lines), compared with the experimental results (dashed lines).

5. Conclusions

A model system of sliding contact between rough surfaces with third-body particles was experimentally studied. The macroscopic friction properties that resulted from the interaction between the existing third-body particles and the first bodies were investigated in relation to various factors, including local friction, particle size and number, and the particle's relative position between the interfaces.

The study revealed that in the presence of a very high local coefficient of friction at the interfaces, which corresponds to dry contact in the experiments, the particle exhibited pure rolling during the sliding of the first bodies. In this scenario, the normal and tangential forces fluctuated more prominently with larger particles, but the overall macroscopic friction resistance for overcoming sliding did not vary with the particle size. Interestingly, this friction resistance was notably affected by the initial alignment of the surface waviness concerning the particle's position, represented by the phase shift between the two waviness patterns of the elastic bodies. The minimum friction resistance occurs when the particle is initially positioned in the valley of the lower surface waviness and contacts the peak of the upper waviness. An approximate solution based on the Hertzian contact theory for the case without phase shift shows the same trend as the experimental results. Additionally, the macroscopic friction resistance depends solely on the geometry of the surface waviness.

Under lubricated conditions, a starkly different behavior was observed. The low local friction at the interface due to the lubrication facilitated the rapid movement of the particle into the valley of the surface waviness upon compression. This abrupt displacement caused the particle to settle into a stable position, necessitating substantial force to push it further. This process is similar to the well-known Prandtl–Tomlinson model suggested by Prandtl in 1928 [21,22]. In this lubricated scenario, the macroscopic friction resistance remained consistent, independent of the initial alignment of the waviness, consistently maintaining the highest level observed in dry contact. Consequently, it can be concluded that lubrication increases the macroscopic friction resistance.

References

1. Popov, V.L. Is Tribology Approaching Its Golden Age? Grand Challenges in Engineering Education and Tribological Research. *Front. Mech. Eng.* **2018**, *4*, 16. [CrossRef]
2. Gates, J.D. Two-body and three-body abrasion: A critical discussion. *Wear* **1998**, *214*, 139–146. [CrossRef]
3. Vakis, A.I.; Yastrebov, V.A.; Scheibert, J.; Nicola, L.; Dini, D.; Minfray, C.; Almqvist, A.; Paggi, M.; Lee, S.; Limbert, G.; et al. Modeling and simulation in tribology across scales: An overview. *Tribol. Int.* **2018**, *125*, 169–199. [CrossRef]
4. Denape, J. Third Body Concept and Wear Particle Behavior in Dry Friction Sliding Conditions. *Key Eng. Mater.* **2015**, *640*, 1–12. [CrossRef]
5. He, G.; Müser, M.H.; Robbins, M.O. Adsorbed layers and the origin of static friction. *Science* **1999**, *284*, 1650–1652. [CrossRef] [PubMed]
6. Jourani, A.; Bouvier, S. Friction and Wear Mechanisms of 316L Stainless Steel in Dry Sliding Contact: Effect of Abrasive Particle Size. *Tribol. Trans.* **2015**, *58*, 131–139. [CrossRef]
7. Bilz, R.; de Payrebrune, K.M. Investigation of the influence of velocity in a tribological three-body system containing a single layer of rolling hard particles from a mechanical point of view. *Tribol. Int.* **2021**, *159*, 106948. [CrossRef]
8. Yousif, B.F.; Nirmal, U.; Wong, K.J. Three-body abrasion on wear and frictional performance of treated betelnut fibre reinforced epoxy (T-BFRE) composite. *Mater. Des.* **2010**, *31*, 4514–4521. [CrossRef]
9. Zum Gahr, K.H. Wear by hard particles. *Tribol. Int.* **1998**, *31*, 587–596. [CrossRef]
10. Schroeder, C.; Grupp, T.M.; Fritz, B.; Schilling, C.; Chevalier, Y.; Utzschneider, S.; Jansson, V. The influence of third-body particles on wear rate in unicondylar knee arthroplasty: A wear simulator study with bone and cement debris. *J. Mater. Sci. Mater. Med.* **2013**, *24*, 1319–1325. [CrossRef]
11. Brink, T.; Milanese, E.; Molinari, J.F. Effect of wear particles and roughness on nanoscale friction. *Phys. Rev. Mater.* **2022**, *6*, 013606. [CrossRef]
12. Hsia, F.C.; Elam, F.M.; Bonn, D.; Weber, B.; Franklin, S.E. Wear particle dynamics drive the difference between repeated and non-repeated reciprocated sliding. *Tribol. Int.* **2020**, *142*, 105983. [CrossRef]
13. Zhang, Y.; Wei, D.; Wu, B.; Jiang, P. Construction of Friction Model of the Third Body Layer and Its Effects on the Dynamic Characteristics in Brake System. *ASME J. Comput. Nonlinear Dynam.* **2023**, *18*, 011003. [CrossRef]
14. Aghababaei, R.; Warner, D.H.; Molinari, J.F. Critical length scale controls adhesive wear mechanisms. *Nat. Commun.* **2016**, *7*, 11816. [CrossRef] [PubMed]
15. Deng, F.; Tsekenis, G.; Rubinstein, S.M. Simple law for third-body friction. *Phys. Rev. Lett.* **2019**, *122*, 135503. [CrossRef] [PubMed]
16. Li, Q.; Lyashenko, I.A.; Starcevic, J. An experimental study on third-body particle transport in sliding contact. *FU Mech. Eng.* **2021**, *19*, 1–5. [CrossRef]
17. de Payrebrune, K.M.; Schönecker, C.; Antonyuk, S.; Bilz, R.; Krull, F.; Noichl, I.; Ripperger, S.; Strohner, D. Interactions Between Particles and Surfaces. In *Component Surfaces*; Springer Series in Advanced Manufacturing; Aurich, J.C., Hasse, H., Eds.; Springer: Cham, Switzerland, 2024.
18. Bilz, R.; de Payrebrune, K.M. Simplified description of hard particles in tribological systems using statistical sample particles. *Proc. Appl. Math. Mech.* **2023**, *23*, e202300106. [CrossRef]
19. Horng, J.; Yu, C.; Chen, Y. Tribological Characteristics and Load-Sharing of Point-Contact Interface in Three-Body Mixed Lubrication. *ASME J. Tribol.* **2022**, *144*, 052201. [CrossRef]
20. Popov, V.L.; Li, Q.; Lyashenko, I.A.; Pohrt, R. Adhesion and friction in hard and soft contacts: Theory and experiment. *Friction* **2021**, *9*, 1688–1706. [CrossRef]
21. Prandtl, L. Ein Gedankenmodell zur kinetischen Theorie der festen Körper. *Z. Angew. Math. Mech.* **1928**, *8*, 85–106. [CrossRef]
22. Popov, V.L.; Gray, J.A.T. Prandtl-Tomlinson model: History and applications in friction, plasticity, and nanotechnologies. *Z. Angew. Math. Mech.* **2012**, *92*, 683–708. [CrossRef]